Techno-Economic Feasibility of Selective CO2 Capture Processes from Biogas Streams using Ionic Liquids as Physical Absorbents

Published in:
Energy & Fuels

Document Version:
Publisher's PDF, also known as Version of record

Queen's University Belfast - Research Portal:
Link to publication record in Queen's University Belfast Research Portal

Techno-Economic Feasibility of Selective CO_2 Capture Processes from Biogas Streams Using Ionic Liquids as Physical Absorbents

Pelayo García-Gutiérrez,*,[†] Johan Jacquemin,*,[‡] Corina McCrellis,[‡] Ioanna Dimitriou,[†] S. F. Rebecca Taylor,[‡] Christopher Hardacre,[‡] and Raymond W. K. Allen[†]

[†]UK Centre for Carbon Dioxide Utilization, Department of Chemical and Biological Engineering, University of Sheffield, Mappin Street, Sheffield, S1 3JD, United Kingdom

[‡]QUILL, School of Chemistry and Chemical Engineering, Queen's University Belfast, Belfast, BT9 5AG, Northern Ireland, United Kingdom

S *Supporting Information*

ABSTRACT: Biogas from anaerobic digestion of sewage sludge is a renewable resource with high energy content, which is composed mainly of CH_4 (40−75 vol %) and CO_2 (15−60 vol %). Other components, such as water (H_2O, 5−10 vol %) and trace amounts of hydrogen sulfide and siloxanes, can also be present. A CH_4-rich stream can be produced by removing the CO_2 and other impurities so that the upgraded biomethane can be injected into the natural gas grid or used as a vehicle fuel. The main objective of this paper is to assess the technical and economic performance of biogas upgrading processes using ionic liquids that physically absorb CO_2. The simulation methodology is based on the COSMO-SAC model as implemented in Aspen Plus. Three different ionic liquids, namely, 1-ethyl-3-methylimidazolium bis[(trifluoromethyl)sulfonyl]imide, 1-hexyl-3-methylimidazoliumbis[(trifluoromethyl)sulfonyl]imide, and trihexyl(tetradecyl)phosphonium bis[(trifluoromethyl)sulfonyl]-imide, are considered for CO_2 capture in a pressure-swing regenerative absorption process. The simulation software Aspen Plus and Aspen Process Economic Analyzer is used to account for mass and energy balances as well as equipment cost. In all cases, the biogas upgrading plant consists of a multistage compressor for biogas compression, a packed absorption column for CO_2 absorption, a flash evaporator for solvent regeneration, a centrifugal pump for solvent recirculation, a preabsorber solvent cooler, and a gas turbine for electricity recovery. The evaluated processes are compared in terms of energy efficiency, capital investment, and biomethane production costs. The overall plant efficiency ranges from 71 to 86%, and the biomethane production cost ranges from $9.18−11.32 per GJ (LHV). A sensitivity analysis is also performed to determine how several technical and economic parameters affect the biomethane production costs. The results of this study show that the simulation methodology developed can predict plant efficiencies and production costs of large scale CO_2 capture processes using ionic liquids without having to rely on gas solubility experimental data.

1. INTRODUCTION

Biogas from anaerobic digestion of biodegradable material, such as sewage sludge or municipal solid waste (MSW), consists primarily of methane (CH_4, 40−75 vol %) and carbon dioxide (CO_2, 15−60 vol %). Other components, such as water (H_2O, 5−10 vol %), trace amounts of hydrogen sulfide (H_2S, 0.005−2 vol %), siloxanes (0−0.02 vol %), and other compounds, may also be present in the biogas. The actual composition of the biogas depends on the type of biodegradable material and the digestion conditions.[1] Because of the high energy content of biogas (∼37 MJ m^{-3}),[2] it can be valorized in different ways, such as heat, electricity generation, and vehicle fuel.

CO_2 and other impurities can be removed from biogas so that an enriched methane stream is produced, which has a higher energy content than raw biogas.[3] This upgraded biomethane can be used as a substitute for natural gas, which can be injected into the natural gas grid or used as a vehicle fuel.[4,5] More recently, it has been suggested that biogas can be further valorized by converting the isolated CO_2 stream into valuable products through carbon dioxide utilization (CDU).[6] Biogas is an important energy source for CDU processes because it could be used either for providing the necessary amount of hydrogen for a CO_2 hydrogenation-to-fuels process via steam reforming of methane or for supplying the necessary process heat and electricity by means of combined heat and power (CHP). It is, however, beyond the scope of this work to consider the captured CO_2 stream for further conversion.

Currently, the most advanced large scale CO_2 capture technologies that can produce an enriched stream of CO_2 are based on amine solvents such as monoethanolamine (MEA).[7−9] The advantages of using such solvents rely on the fact that they offer a high CO_2 absorption capacity (up to 2 mol of MEA for 1 mol of CO_2 under ambient conditions). However, they are generally prone to evaporate, liable to be corrosive at elevated temperatures, and expensive to regenerate due to the high energy penalty.[9−11] In recent years, alternative materials have been suggested for CO_2 capture, including KS-1 solvent, Econamine FG^{+SM}, ionic liquids, amidoxim, metal−organic frameworks, microporous organic polymers, and zeolitic imidazolate frameworks and membranes, among others.[12]

Ionic liquids (ILs) are among the class of novel solvents that have high CO_2 affinity and therefore have attracted significant attention in the last several years.[12,13] They offer a number of advantages over amine-based solvents, such as their extremely low vapor pressure, which prevents the solvent from being released to the atmosphere, and their low corrosivity.[12,14] Furthermore, the vast number of possible combinations of cations and anions allows the solvent to be custom-made for specific applications.[15]

It is known that a potential IL candidate for CO_2 capture processes must possess a high CO_2 affinity, significant pressure/temperature dependence of CO_2 solubility, and high selectivity toward CO_2 solubility over other components present in the gas mixture, such as CH_4, N_2, H_2, H_2S, and so forth.[15] Consequently, many studies have focused on these desirable properties of the IL candidate, either experimentally or through mathematical modeling; however, just a few studies[16−19] have focused on whole-scale process analysis, which is essential if serious effort is to be made to consider commercial implementation of this technology.

This is the topic of this paper, which examines the techno-economic feasibility of selective CO_2 capture processes from biogas streams using ILs as physical absorbents. The isolated CH_4 is considered to be injected into the natural gas grid, whereas the isolated CO_2 stream can be either stored underground or converted into valuable products, such as commodity chemicals, polymers, and fuels.[20] The aim of this study is to use COSMO-based thermodynamic models in Aspen Plus to assess IL-based biogas upgrading processes in terms of process efficiency and cost. The simulation methodology has been extensively used by other researchers[21−25] to evaluate a variety of separation processes; however it has not been used before to assess biogas upgrading processes. The methodology allows estimation of physical properties of the ILs as well as the solubility of the gaseous species (CO_2 and CH_4). Furthermore, it can be used as a basis for further research in the field because it considers ILs made of any combination of cation and anion as well as different gas streams.

A description of the processes evaluated in this work is presented in the next section. Section 3 outlines the methodology for process modeling followed by section 4, which details the methodology for cost estimation. Section 5 comprises a discussion of the results, followed by the main conclusions of this work in section 6.

2. PROCESS DESCRIPTION

2.1. Process Overview. The target application considered in this study is biogas upgrading (up to 95 vol % CH_4) using ILs that selectively absorb CO_2 physically. Three different processes have been developed with each of them employing a different IL. The design of the three processes is identical, differing only in the type of IL used; this allows for a fair comparison between the evaluated processes in terms of energy requirements, solvent capacity, solvent loss, and cost.

The flow diagram of the biogas upgrading plant is shown in Figure 1. It is a pressure-swing regenerative process based on the one suggested by Shiflett et al.[19] The process considered by Shiflett et al. and the one presented in this work only differ in a heat exchanger not being included in this work's process with the reason being that in this work the IL is regenerated solely by pressure swing, i.e., there is no need of a heat supply to regenerate the IL. The process consists of a multistage compressor, a packed absorption column for CO_2 absorption,
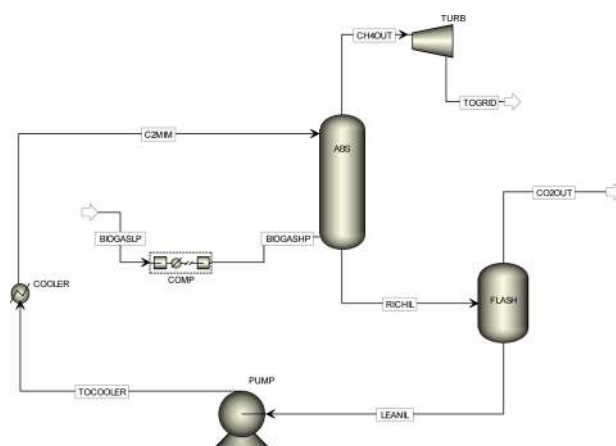

Figure 1. Process flow diagram of the biogas upgrading plant.

a flash evaporator for solvent regeneration, a centrifugal pump for solvent recirculation, a preabsorber solvent cooler, and a gas turbine for electricity recovery.

The biogas generated from anaerobic digestion of sewage sludge in a waste water treatment plant (WWTP) is compressed from atmospheric pressure to the column's operating pressure of 30 bar in a multistage gas compressor with intercooling. The composition of the biogas is 35 vol % of CO_2 and 65 vol % of CH_4. It is assumed that neither NH_3 nor H_2S are present in the biogas because ammonia is not produced when sewage sludge is employed as the feedstock and hydrogen sulfide is produced at ppb levels.[6] Although crude biogas produced at WWTPs is usually saturated with water, this work assumes that a drying pretreatment that removes the water in the crude biogas has been carried out prior to feeding it to the compressor.[26] The biogas is produced by the WWTPs anaerobic digester[27] at a rate of 3,775 kg h^{-1}.

The compressed biogas at 15 °C and 30 bar is fed counter-currently in the packed absorption column with the IL at 15 °C and 30 bar, which selectively absorbs CO_2 in the biogas to form a CO_2-rich IL solution. The upgraded biomethane stream lean in CO_2 (95 vol % of CH_4) is released from the top of the absorber whereas the IL solution rich in CO_2 is fed into a flash drum. The IL is regenerated in the flash drum by a pressure swing, i.e., reducing its pressure to 0.01 bar. It is then recycled back by the centrifugal pump to the absorption column for reuse, whereas the concentrated CO_2 stream is released from the top of the flash drum. It should be noted that, as this is a pressure-swing capture process, an external supply of heating is not involved in any of the unit operations.

2.2. Ionic Liquid Selection. The three ILs selected to act as physical absorbents for CO_2 capture are 1-ethyl-3-methylimidazolium bis[(trifluoromethyl)sulfonyl]imide, 1-hexyl-3-methylimidazolium bis[(trifluoromethyl)sulfonyl]-imide, and trihexyl(tetradecyl)phosphonium bis-[(trifluoromethyl)sulfonyl]imide. Their molecular structures are depicted in Figures 2−4, respectively.

The three ILs have the same anion, namely, bis-[(trifluoromethyl)sulfonyl]imide ($[Tf_2N]^-$), and are based on three different cations: two 1-alkyl-3-methylimidazolium ($[C_nMIm]^+$ with n = 2 or 6) and trihexyl(tetradecyl)-phosphonium ($[P_{66614}]^+$). The bis{(trifluoromethyl)sulfonyl}-imide anion has been selected as ILs based on this anion have a high affinity for CO_2 capture[28] compared with those based on, for instance, the hexafluorophosphate ($[PF_6]^-$) anion.[29]
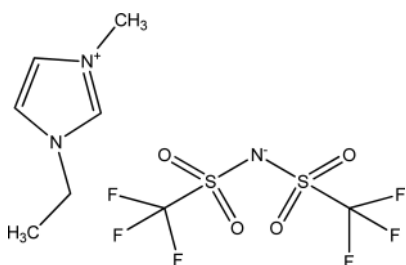
Figure 2. 1-Ethyl-3-methylimidazolium bis[(trifluoromethyl)sulfonyl]-imide ([C₂MIm][Tf₂N]).
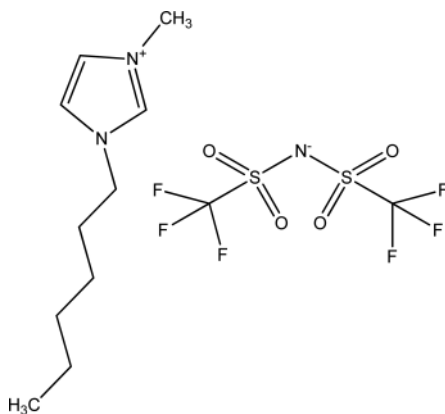
Figure 3. 1-Hexyl-3-methylimidazolium bis[(trifluoromethyl)-sulfonyl]imide ([C₆MIm][Tf₂N]).
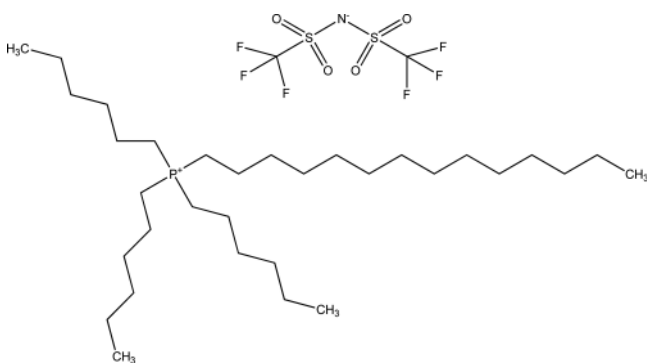
Figure 4. Trihexyl(tetradecyl)phosphonium bis[(trifluoromethyl)-sulfonyl]imide ([P₆₆₆₁₄][Tf₂N]).

Imidazolium cations have been selected because they are very well reported in the literature and their structure presents an unsaturated ring (i.e., the positive charge is mainly delocalized on the cation structure) a contrario of the phosphonium cation where the charge is mainly localized on the phosphorus atom. Conversely, the selected phosphonium cation has an acyclic structure containing very large alkyl chain lengths that increase the cohesive energy of this cation in comparison with the selected imidazolium cations. In fact, van der Waal's forces are higher in the phosphonium cation than in the selected imidazolium cations, in contrast to the Coulombic forces. In other words, this particular selection of cations allows investigation of how cation structure and cation–anion interactions impact CO_2 uptake, process modeling, and the cost.

Furthermore, these ILs have been chosen as solvents for selective CO_2 capture in this study as they rely on their high CO_2 affinity and CO_2/CH_4 selectivity[12,15,30,31] as well as on the availability of data regarding pure component physical properties.[32]

3. MODELING METHODOLOGY

3.1. Modeling Overview. The process flowsheets of the three biogas upgrading plants studied were developed using Aspen Plus as the process simulation software, which enabled the estimation of mass and energy balances as well as utility requirements. These calculations were then used as the inputs for the techno-economic assessments.

3.1.1. Property Method. The conductor-like screening model with segment activity coefficient (COSMO-SAC) property method as implemented in Aspen Plus has been used to model the different unit operations present in this study as well as to calculate the physical and thermodynamic properties of the pure components and mixtures. This model is a robust preliminary tool for fast screening and design of ILs for CO_2 capture as it readily provides relevant information on gas–liquid interactions without having to rely on binary interaction parameters or experimental data,[15,30,33,34] which often consumes time and resources. COSMO-SAC is a solvation model that describes the electrical interactions in the molecular surface of polarizable species (Aspen Technology, 2013).[35] Although it requires complex quantum mechanics calculations, they only have to be done once for a particular molecule, after which the results can be stored. Unlike other activity coefficient models, such as UNIFAC or UNIQUAC, individual atoms are used for phase equilibria as the building blocks instead of functional groups. This enables the COSMO-SAC model to be more flexible as it can be applied to a wider range of systems, for instance, complex molecules such as the ILs considered in this study, which are not present in the Aspen Plus database.

The solubility of a gas in a solvent is determined using eq 1 by assuming identical fugacity of the gas in both the vapor and liquid phases[15]

$$y_i P \bar{\phi}_i = P_i = x_i \gamma_i(T, P, x) f_i(T, P) \qquad (1)$$

where x_i and y_i are the mole fractions of the gas in the vapor and liquid phases, respectively, P the total pressure of the system, P_i the partial pressure of the gas, $\bar{\phi}_i$ the fugacity coefficient in the vapor phase, γ_i the activity coefficient in the liquid phase, and f_i the fugacity of the gas molecule (CO_2 and CH_4 in this study) in a hypothetical liquid state at pressure P and temperature T. Given the extremely low vapor pressure of the liquids (i.e., $y_i = 1$) considered in this study,[12,13] the range of temperature and pressure, as well as the nature of the gaseous species (CO_2 and CH_4), it can be assumed that the fugacity of a gas molecule in its liquid state could be estimated by its vapor pressure at a temperature away from its critical point.[15] The fugacity and the fugacity coefficient were both determined directly using Aspen Plus, and thus the solubilities of the gas in the liquid phase (x_i) were directly calculated within Aspen at a given pressure P, temperature T, and partial pressure of the gas P_i by using eq 2

$$P \bar{\phi}_i = x_i \gamma_i(T, P, x) f_i(T, P) \qquad (2)$$

The COSMO-SAC model calculates the liquid activity coefficient γ_i following eq 3

$$\ln \gamma_i = \frac{A_i}{a_{\text{eff}}} \sum_{\sigma_m} p_i(\sigma_m)[\ln \Gamma_S(\sigma_m) - \ln \Gamma_i(\sigma_m)] + \ln \gamma_i^{SG}$$

(3)

where A_i is the molecular surface area of component i, a_{eff} the standard segment surface area, $p_i(\sigma_m)$ the sigma profile of component i, $\Gamma_S(\sigma_m)$ the segment activity coefficient of segment σ_m in the solvent mixture, $\Gamma_i(\sigma_m)$ the segment activity coefficient of segment σ_m in component i, and γ_i^{SG} the Staverman–Guggenheim model for combinatorial contribution to γ_i.

In the COSMO-SAC model, the probability distribution of surface charge density, called the sigma profile $p_i(\sigma_m)$, describes the electronic nature of the molecule studied as reported in eq 4

$$p_i(\sigma_m) = \frac{A_i(\sigma_m)}{A_i}$$

(4)

It must be noted that, in Aspen Plus, the COSMO-SAC model does not require binary parameters to account for the interaction between components, but it requires six input parameters that are genuine of the COSMO-SAC model for each component.[21−25] The first parameter called *CSACVL* is the component volume parameter, which is always defined in cubic angstroms. The remaining parameters *SGPRF1−SGPRF5* are five molecular component sigma profile parameters. All six input parameters are obtained using the conductor-like screening model for real solvents (COSMO-RS) methodology. In this study, the COSMOthermX program[36] is used to perform the COSMO-RS calculations and thus obtain the parameters *SGPRF1−SGPRF5* as well as *CSACVL*. A detailed explanation on how the COSMO calculations were performed can be found in section 3.2.2. In addition to these six genuine parameters, the COSMO-SAC model requires a set of pure component physical properties as detailed in section 3.2.1. The following sections describe in detail the Aspen Plus implementation of the different unit operations that are included in the biogas upgrading plant.

3.1.2. Biogas Compressor. Biogas is produced by the anaerobic digester plant at atmospheric pressure. Because the packed absorber operates at 30 bar (see section 2.1), biogas needs to be compressed to the absorber's operating pressure to enhance the absorption process. A multistage centrifugal compressor with intercooling was used for the compression of biogas, which was modeled using the Aspen *MCompr* subroutine. The specifications of the compressor are shown in Table 1.

The compression type was chosen to be isentropic with an isentropic efficiency of 0.72, which is the default value in Aspen Plus. The rigorous ASME calculation method was used because it provides the most accurate results.[37] Once the isentropic calculations were carried out, the process flowsheet was

Table 1. Biogas Compressor Specifications

specification	value
number of stages	3
compression type	isentropic using ASME method
discharge pressure (bar)	30
isentropic efficiency (default)	0.72
intercooling outlet temperature (°C)	120
outlet temperature from last stage (°C)	15

implemented in Aspen Process Economic Analyzer (APEA), which calculated the compressor driver efficiency given the compression conditions and compressor type. APEA then calculated the electrical power of the compressor driver using both the isentropic and driver efficiencies. This actual compressor electrical consumption was the value used for the estimation of the total electrical power consumption in the plant. Intercooling was required to decrease the temperature of biogas to the absorber operating temperature (15 °C).

3.1.3. Absorption Column. The packed absorber is fed with biogas from the bottom and the IL from the top, which flow in a counter-current pattern. At the given operating conditions, the IL solution absorbs the most soluble gas, in this case CO_2, leaving the bottom of the column as a CO_2-enriched solution. The gas stream lean in CO_2 leaves the absorber from the top. The absorption column was modeled in Aspen Plus with the RadFrac subroutine, which is suitable for modeling a wide range of vapor–liquid fractionation processes.[37] The specifications for the packed absorber, as implemented in Aspen Plus, are summarized in Table 2.

Table 2. Specifications of the Packed Absorption Column

specification	value
number of theoretical stages	5
calculation type	rate-based
condenser	none
reboiler	none
convergence algorithm	sum-rates
pressure drop (bar)	0.5
packing type	Pall rings (1 in.)
column diameter (m)	1.2
packing height (m)	20

It must be noted that the number of theoretical stages was the minimum possible at which the model converged. Any further increase in the number of theoretical stages did not result in any improvement in performance. A design specification is used to obtain the desired CH_4 concentration of 95 vol % in the upgraded biomethane stream by adjusting the flow rate of IL fed into the column.

Pall rings were used in the absorber as the type of packing, which have been considered by others for similar CO_2 capture processes using ILs as physical absorbents.[16,17] Although high area-related liquid loads are used in the absorption column, they are within the packing manufacturers' operating range.[38,39] Random packing was chosen due to its lower cost and better liquid distribution,[40] especially when using high viscosity liquids such as the ILs studied in this work. With respect to the high viscosity of the ionic liquids, it should be noted that Aspen Plus performs a hydraulic analysis of the absorber to ensure optimum mass transfer and flow within the absorber. The liquid and vapor phase binary mass transfer coefficients as well as the total interfacial area for mass transfer were estimated using the Billet and Schulte's correlation, which provides good estimates of mass transfer-related parameters over a wide range of packing types, sizes, and operating conditions.[41]

The liquid and vapor phase binary mass transfer coefficients $k_{i,k}^L$ and $k_{i,k}^V$, respectively are defined by Billet and Schulte as reported in eqs 5 and 6

$$k_{i,k}^L = C_L \left(\frac{g\rho_t^L}{\mu^L} \right)^{0.167} \sqrt{\frac{D_{i,k}^L}{d_h}} \left(\frac{u_s^L}{a_p} \right)^{0.333} \tag{5}$$

$$k_{i,k}^V = C_V \left(\frac{1}{\sqrt{\varepsilon - h_t}} \right) \sqrt{\frac{a_p}{d_h}} D_{i,k}^V Re_V^{0.75} Sc_{Vi,k}^{0.333} \tag{6}$$

where C_L and C_V are the mass transfer coefficient parameters for liquid and vapor, respectively, and depend on the shape and structure of the packing, g the gravitational gravity, ρ_t^L the density of the liquid, μ^L the viscosity of the liquid, $D_{i,k}^L$ and $D_{i,k}^V$ the diffusivity of the liquid and vapor, respectively, d_h the hydraulic diameter, u_s^L the superficial velocity of the liquid, a_p the specific area of the packing, ε the void fraction of the packing, h_t the fractional holdup, and Re_V and $Sc_{V\,i,k}$ the Reynolds and Schmidt numbers for the vapor, respectively.

The total interfacial area for mass transfer a^I is defined by eq 7 as

$$a^I = a_e A_t h_p \tag{7}$$

where A_t is the cross-sectional area of the column, h_p the height of the packed section, and a_e the effective surface area per unit volume of the column. The latter is calculated using eq 8

$$a_e = a_p \frac{1.5}{\sqrt{a_p d_h}} \left(\frac{u_s^L d_h \rho_t^L}{\mu^L} \right)^{-0.2} \left(\frac{(u_s^L)^2 \rho_t^L d_h}{\sigma} \right)^{0.75} \left(\frac{(u_s^L)^2}{g d_h} \right)^{-0.45} \tag{8}$$

where σ is the liquid surface tension.

3.1.4. Upgraded Biomethane Turbine. The upgraded biomethane stream lean in CO_2 that leaves the top of the packed absorber at high pressure (29.5 bar, assuming 0.5 bar pressure drop across the column) is fed into a turbine, which extracts energy from the stream at high pressure and converts it into useful work. The turbine was modeled in Aspen Plus using the *Compr* model with the turbine calculation type. As with the biogas compressor, the compression type was chosen to be isentropic with an isentropic efficiency of 0.72, which is the default value in Aspen Plus. Similarly, the electrical output of the generator coupled to the turbine was calculated by Aspen process economic analyzer (APEA) at the given process conditions and turbine type.

3.1.5. Regeneration Flash Evaporator. The process concepts considered in this work employ the pressure swing solvent regeneration option whereby physical absorption is carried out at high pressure, whereas the regeneration of the solvent (desorption of the gases) takes place at pressures below atmospheric pressure. The IL-rich solution leaves the bottom of the packed absorber at high pressure and is fed into the adiabatic flash evaporator (flash drum) where the solution undergoes a reduction in pressure (from 29.5 to 0.01 bar). The liquid settles to the bottom of the vessel due to gravity, and the vapor escapes through the top of the vessel.

3.1.6. Solvent Recirculation Pump. As explained in the previous sections, the regenerated IL-lean solution leaves the bottom of the flash evaporator at low pressure (0.01 bar) and needs to be brought back to the column operating pressure of 30 bar. A centrifugal pump is therefore used to pressurize the IL-lean solution back to the absorption column, which was modeled using the Aspen *Pump* subroutine. The pump efficiency was set to 0.7, which is assumed to be a reasonable value for centrifugal pumps.[42] Then, the process flowsheet was

implemented in APEA, which calculated the driver efficiency at the given fluid conditions and pump type. APEA then calculated the electrical power of the pump motor using both the pump and driver efficiencies. This actual motor electrical power was the value used for the estimation of the total electrical power consumption in the plant.

3.1.7. Preabsorber Solvent Cooler. A preabsorber solvent cooler is employed to cool the IL-lean solution back to 15 °C. This cooler needs to be used because the IL solution undergoes an increase in temperature due to the enthalpy of solution when the gases (mostly CO_2) are absorbed into the liquid in the packed absorber. Moreover, following the adiabatic flash evaporation stage, the IL-lean solution is pressurized back to 30 bar from 0.01 bar, which further increases the temperature of the IL-lean solution. The cooler is modeled in Aspen Plus using the *Heater* block.

3.2. Aspen Plus Parameters. *3.2.1. Pure Component Physical Properties.* As the ILs studied in this work are not included in the Aspen Plus component database, pure IL physical properties were retrieved from the literature and implemented in Aspen Plus. Data regression was used to accurately represent important properties in the desired range of pressures and temperatures. It is based on maximum likelihood estimation and processes raw data to determine parameters for physical property models. The estimated parameters and their corresponding models and physical properties are shown in Table S1. ASPEN PLUS input files for the ILs processes are available at: http://dx.doi.org/10.17034/0d628da6-76d8-41b6-a8a9-e75129726a98.

The Britt−Luecke algorithm was used with the Deming initialization method[43] in all three process designs. It should be noted that the PLXANT parameter needed by the extended Antoine equation for the estimation of the liquid vapor pressure was set to the minimum allowable value of -1×10^{-8} in Aspen Plus due to the negligible vapor pressure inherent to ILs.[12,13] The data sources of the ILs' ideal gas heat capacities, liquid densities, and liquid viscosities are given in Table 3.

Table 3. Data Sources of the Ionic Liquids Physical Properties

	$[C_2MIm]$ $[Tf_2N]$	$[C_6MIm][Tf_2N]$	$[P_{66614}]$ $[Tf_2N]$
ideal gas heat capacity	Paulechka et al.[44]	Blokhin et al.[45]	Ferreira et al.[46]
liquid density	Jacquemin et al.[47]	Widegren & Magee[48]	Neves et al.[49]
liquid viscosity	Schreiner et al.[50]	Widegren & Magee[48]	Neves et al.[49]

In addition to the properties shown in Table 3, several scalar physical properties, i.e., nontemperature- or pressure-dependent, were required. These are shown in Tables 4−6. The molecular weights of the ILs were retrieved from the Sigma Aldrich catalogue.[51] The boiling point, critical temperature, critical pressure, critical volume, and acentric factor of the ILs were estimated using the modified Lydersen−Joback−Reid group contribution method proposed by Valderrama y Rojas,[52] which is considered the most robust and common technique for IL critical properties estimation. Finally, the volume parameter of the COSMO-SAC model was calculated using COSMOthermX software.[36]

3.2.2. Sigma Profiles. During this study, the 3D molecular structure optimization of each investigated ion and gas and the

Table 4. Scalar Properties of $[C_2MIm][Tf_2N]$ Ionic Liquid

property	value
molecular weight, g mol^{-1}	391.310
boiling point, K	805.930
critical temperature, K	1244.700
critical pressure, bar	32.610
critical volume, cm^3 mol^{-1}	892.890
acentric factor	0.182
COSMO-SAC volume, $Å^3$	376.700

Table 5. Scalar Properties of $[C_6MIm][Tf_2N]$ Ionic Liquid

property	value
molecular weight, g mol^{-1}	447.420
boiling point, K	897.450
critical temperature, K	1287.000
critical pressure, bar	23.860
critical volume, cm^3 mol^{-1}	1121.330
acentric factor	0.354
COSMO-SAC volume, $Å^3$	464.670

Table 6. Scalar Properties of $[P_{66614}][Tf_2N]$ Ionic Liquid

property	value
molecular weight, g mol^{-1}	764.023
boiling point, K	310.560
critical temperature, K	1586.735
critical pressure, bar	8.513
critical volume, cm^3 mol^{-1}	2423.540
acentric factor	0.892
COSMO-SAC volume, $Å^3$	973.494

generation of their COSMO files were performed using the TURBOMOLE quantum chemistry package[53] and were then visualized using the COSMOthermX software (version C30_1501, COSMO*logic* 2015). The structures were optimized with a convergence criterion of 10^{-8} Hartree in the gas phase. The TURBOMOLE 6.0 package was used for all of the density functional theory (DFT) calculations using the resolution of identity approximation.[54] The B3LYP functional[55] was chosen for geometry optimization, and all calculations were completed with the def-TZVP basis set,[55] combining the RI technique calculations as recommended by COSMO*logic*.[36] The σ-profile for each ion or gas was generated from its COSMO file using COSMOthermX,[36] and the σ-profile for each ionic liquid was determined as the sum of the cation and anion σ-profiles. These sigma profiles were then implemented in Aspen Plus within the COSMO-SAC property method.

For testing the functionality of the modified Aspen databank, the CH_4 and CO_2 solubility data in the selected ILs were modeled first. This choice was made for a number of reasons: First, the single gas solubility in a solvent can be relatively easily calculated in Aspen Plus by simulating an equilibrium flash model. Second, CO_2 and CH_4 solubility data are already reported in the literature[56−60] for the three selected ILs at elevated pressures (data not available for CH_4 in $[P_{66614}]$-$[Tf_2N]$). Third, the COSMO-RS model has previously been used by our group for predicting data of the gas solubility in ILs.[61] Figures S4−S8 show how the solubility data predictions from Aspen Plus correlates with experimental data (when available) for both CO_2 and CH_4 in the three ILs. In general, the Aspen predictions compare reasonably well in terms of average relative deviation (ARD) with experimental data

(10.35−27.23% ARD for CO_2 and 26.72−36.14% ARD for CH_4). These ARD values are in the range of those reported by other authors using COSMO calculations for gas solubility predictions in ILs.[15] Only at elevated pressure (above the IL's critical pressure) do the COSMO-SAC model predictions start to deviate considerably from the experimental values. Table 7 shows the equilibrium absorption capacity of each ionic liquid at the absorber's operating conditions (15 °C and 30 bar) predicted by the COSMO-SAC model in Aspen Plus.

Table 7. ILs Absorption Capacities As Predicted by the COSMO-SAC Model

	x_{CO_2}	mol CO_2/kg IL
$[C_2MIm][Tf_2N]$	0.661	4.98×10^{-3}
$[C_6MIm][Tf_2N]$	0.712	5.53×10^{-3}
$[P_{66614}][Tf_2N]$	0.840	6.87×10^{-3}

4. COST ESTIMATION METHODOLOGY

The capital and operating costs of the three biogas upgrading plants considered in this study were estimated to identify the most promising process in terms of cost of upgraded biomethane. The assumptions for the economic evaluation as well as the price of the utilities used in the processes are summarized in Table 8.

Table 8. General Economic Parameters and Utility Prices

General Economic Parameters	
base year	2013
plant life, years	20
plant annual operating hours	8000
loan interest rate	10%
Utility Prices	
electricity, $ kWh^{-1}	0.1108
refrigerant, $ t^{-1}	0.2431

It must be noted that biogas, which is the feedstock for the three evaluated process concepts, has no cost because it is assumed that the upgrading plant is part of a large wastewater treatment plant that produces biogas from anaerobic digestion of primary and secondary sludge.

In techno-economic assessments, it is required to determine the capital costs, which is the total investment needed to finance the project to the point at which the plant is ready to operate. A method based on the percentage of delivered-equipment cost (DEC)[62] was used in this study to estimate the capital costs as shown in Table 9. The software Aspen process economic analyzer (APEA), licensed by Aspen Tech,[63] was used to determine the DEC of each biogas upgrading plant.

The IL cost in Table 9 represents the cost of the IL fluid assuming that it is not replaced throughout the life of the plant (no evaporation or degradation losses). The selling prices of ILs are highly dependent on the type of cation and anion, the manufacturer, as well as the scale of production of the IL used. At the current IL production scale, one can expect that their selling price will be high; however, several authors[65−67] agree that bulk ionic liquids (the ones consumed in large scale applications) could be sold at prices between €10−30 per kg in the near future with production on a large scale (at least one ton). In this work, a selling price of $34 kg^{-1} (€30 kg^{-1}) for all the three ILs considered is used.

Table 9. Ratio Factors for Total Capital Investment Estimation

total capital investment	
Direct Cost	% of DEC
purchased equipment	100
equipment installation	47
instrumentation and control	36
piping	68
electrical	11
building and building services	18
yard improvements	10
service facilities	70
total direct cost (TDC)	360
Indirect Cost	% of DEC
engineering	33
construction expenses	41
legal costs	4
contractor's fee	22
contingency	44
total indirect cost (TIC)	144
fixed capital invest. (FCI) = TDC + TIC	504
working capital	15% of TCI
IL cost	
total capital invest. (TCI) = TDC + TIC + working capital + IL cost	

The capital investment needed to carry out a project is usually borrowed and then repaid annually over the lifetime of the plant at a given interest. In this study, a 10% interest rate is assumed. The annual amount required to repay the loan on capital costs is given by Dimitriou et al.[6] as reported in eq 9

$$A = \text{TCI} \frac{r(1 + r)^N}{(1 + r)^N - 1} \tag{9}$$

where A is the annuity of the capital investment, TCI the total capital investment as estimated in Table 9, r the interest rate, and N the lifetime of the project.

The total annual costs consist of capital investment annuities as well as operating costs, i.e., fixed charges, direct production costs, general expenses, and plant overhead. The plant operating costs were estimated using the method summarized in Table 10, which was adapted from Peters et al.[62]

The biogas production costs are calculated by dividing the total annual costs by the amount of upgraded biomethane produced in a year. For making a straightforward comparison between the three evaluated ILs, the price inflation of equipment and raw materials are not included in the annual costs. Similarly, government subsidies such as the Renewable Heat Incentive (RHI) in the UK[64] are not considered in this study.

5. RESULTS

5.1. Mass and Energy Balances. The mass and energy balances for the three process concepts considered in this study are presented in Table 11. For a fair comparison between the different concepts, the mass flow and energy content of the biogas are identical in all cases. Similarly, the CH_4 concentration in the biomethane stream is 95 mol % in all cases. With regard to the process energy flows, Table 11 includes both the lower heating value of the material streams coming in and out of the three processes as well as the electricity inputs and outputs. Apart from biogas and electricity, there are no other energy inputs, e.g., heat. The process

Table 10. General Assumptions for Operating Cost Estimation

operating costs	
Fixed Charge	
local taxes	2% of FCI
insurance	1% of FCI
Direct Prod. Cost[a]	
maintenance (M)	7% of FCI
operating labor (OL)[b]	$29 h^{-1}
supervision (S)	15% of OL
operating supplies	15% of M
laboratory charges	15% of OL
plant overhead	15% of (M + OL + S)
General Expenses	
administrative cost	15% of OL
distribution and marketing	2% of OPEX
R&D cost	2% of OPEX

[a]Utility costs are also included in the direct production cost. [b]Hourly wages taken from APEA; 40 man-hours/day are assumed for the given plant capacity.[55]

Table 11. Summary of the Mass and Energy Balances of the Evaluated Processes

	$[C_2MIm]$ $[Tf_2N]$	$[C_6MIm]$ $[Tf_2N]$	$[P_{66614}]$ $[Tf_2N]$
ionic liquid required (kg h^{-1})	56,998	52,745	44,182
Plant Inputs			
biogas (kg h^{-1})	3775	3775	3775
biogas (kW) (LHV)	23,454	23,454	23,454
electricity (kW)	545	575	595
Plant Outputs			
biomethane (kg h^{-1})	1522	1455	1264
biomethane (kW) (LHV)	20,474	19,570	16,997
electricity (kW)	74	70	61
IL capacity (kg IL/kg BM)	38	36	35
energy yield, %	87	83	73
energy efficiency, %	86	82	71

concept using the $[C_2MIm][Tf_2N]$ IL produces 1522 kg h^{-1} of biomethane at 95 mol %, followed by 1455 and 1264 kg h^{-1} produced by the second and third concepts. The difference in the biomethane output produced by each process concept can be explained by the fact that, although the $[C_6MIm][Tf_2N]$ and $[P_{66614}][Tf_2N]$ ILs have a higher CO_2 absorption capacity, as shown in Table 7, they also absorb more CH_4 than $[C_2MIm][Tf_2N]$. For these amounts of biomethane to be produced, 56,998 kg h^{-1} of $[C_2MIm][Tf_2N]$, 52,745 kg h^{-1} of $[C_6MIm][Tf_2N]$, and 44,182 kg h^{-1} of $[P_{66614}][Tf_2N]$ are needed. These results demonstrate that the $[P_{66614}][Tf_2N]$ has the highest CO_2 absorption capacity, followed by $[C_6MIm]$-$[Tf_2N]$ and $[C_2MIm][Tf_2N]$, which is in agreement with experimental data.[56,58,60]

Considering the electricity flows, it should be noted that the values presented in Table 11 account for both the biogas compressor and the pump recirculation. In all cases, the biogas compressor consumed 500 kW. The pump in the first process concept needs 45 kW of electricity, whereas the pumps in the second and third concepts require 75 and 95 kW, respectively; therefore, the biogas compressor accounts for the vast majority of the plant electricity consumption. These results show that

the viscosity of the IL has a significant effect on the amount of electricity used by the recirculation pump.

5.2. Energy Yields and Efficiencies. The energy yields and efficiencies of the evaluated processes are also presented in Table 11. The energy yield, Y_E, is a measure of the energy content of biogas on an LHV basis that ends up in the upgraded biomethane and is given by eq 10

$$Y_E = \frac{M_{biomethane} \cdot LHV_{biomethane}}{M_{biogas} \cdot LHV_{biogas}} \quad (10)$$

Eq 10 shows that high biomethane production results in high energy yields; therefore, the highest energy yield is achieved by $[C_2MIm][Tf_2N]$ (87%), followed by $[C_6MIm][Tf_2N]$ (83%) and $[P_{66614}][Tf_2N]$ (73%).

As reported in eq 11, the energy efficiency, η_E, takes into account the total energy input to the plant, i.e., biogas and electricity, and the total energy output from the plant, i.e., biomethane and electricity

$$\eta_E = \frac{(M_{biomethane} \cdot LHV_{biomethane}) + \text{electricity produced}}{(M_{biogas} \cdot LHV_{biogas}) + \text{electricity consumed}} \quad (11)$$

Similar to the results of the energy yield, the process using $[C_2MIm][Tf_2N]$ has the highest energy efficiency, achieving a value of 86%. The reason for this is that in addition to the increased biomethane production of the $[C_2MIm][Tf_2N]$ process (which leads to an increased electricity production in the turbine), it also needs less electricity for IL recirculation, because of its lower viscosity. The second most efficient process in terms of energy efficiency is $[C_6MIm][Tf_2N]$ (82%), followed by the more viscous IL investigated in this work, i.e. $[P_{66614}][Tf_2N]$ with a value of 71%.

5.3. Economic Analysis. Table 12 shows the breakdown of the capital costs related to each process concept using the method described in Table 9. The total capital investment costs for the three process concepts are $15.2 million for

Table 12. Summary of the Total Capital Investment

	$[C_2MIm]$ $[Tf_2N]$ (M\$)	$[C_6MIm]$ $[Tf_2N]$ (M\$)	$[P_{66614}]$ $[Tf_2N]$ (M\$)
Direct Cost			
purchased equipment	2.17	2.22	2.25
equipment installation	1.02	1.04	1.06
instrumentation and control	0.78	0.80	0.81
piping	1.48	1.51	1.53
electrical	0.24	0.24	0.25
building and building services	0.39	0.40	0.40
yard improvements	0.22	0.22	0.22
service facilities	1.52	1.55	1.57
Indirect Cost			
engineering	0.72	0.73	0.74
construction expenses	0.89	0.91	0.92
legal costs	0.09	0.09	0.09
contractor's fee	0.48	0.49	0.49
contingency	0.96	0.98	0.99
Other Costs			
working investment	2.28	2.29	2.26
IL cost	1.96	1.81	1.52
TOTAL CAPEX	15.18	15.28	15.10

$[C_2MIm][Tf_2N]$, \$15.3 million for $[C_6MIm][Tf_2N]$, and \$15.1 million for $[P_{66614}][Tf_2N]$. In all cases, the purchased equipment, piping, service facilities, and working investment are the items that contribute more significantly toward the total capital investment. $[C_2MIm][Tf_2N]$ results in lower capital costs due to the fact that the cost of the regeneration pump and the flash evaporator are considerably cheaper than in the other two concepts.

The selling price of the IL fluids is also included in Table 12. $[C_2MIm][Tf_2N]$ results in higher IL costs because it requires more fluid than $[C_6MIm][Tf_2N]$ and $[P_{66614}][Tf_2N]$, as this IL has a lower molar volume and CO_2 uptake than the two other investigated ILs.

The annual operating and maintenance costs, which mainly include expenditures for utilities, labor, maintenance, and tax, are presented in Table 13. The operating costs range from \$3.1

Table 13. Summary of the Operating Costs

	$[C_2MIm]$ $[Tf_2N]$ (M\$)	$[C_6MIm]$ $[Tf_2N]$ (M\$)	$[P_{66614}][Tf_2N]$ (M\$)
Fixed Charge			
local taxes	0.22	0.22	0.23
insurance	0.11	0.11	0.11
Direct Prod. Cost			
cooling	0.08	0.08	0.08
electricity	0.42	0.45	0.47
maintenance	0.77	0.78	0.79
operating labor	0.38	0.38	0.38
supervision	0.06	0.06	0.06
operating supplies	0.11	0.12	0.12
laboratory charges	0.06	0.06	0.06
plant overhead	0.72	0.73	0.74
General Expenses			
administrative cost	0.06	0.06	0.06
distribution and marketing	0.06	0.06	0.06
R&D cost	0.06	0.06	0.06
TOTAL OPEX	3.10	3.18	3.23

to 3.2 million. The process using $[C_2MIm][Tf_2N]$ results in the lowest operating costs due to its lower capital costs as well as its lower electricity consumption. In fact, electricity consumption is one of the main contributors to the operating costs, representing 13−15% of the total O&M. Other large contributors toward the O&M are the operating labor (around 12% in all cases), plant overhead (23−24%), and maintenance (24−25%).

The production costs per GJ of biomethane produced for all cases considered are shown in Table 14. The calculated production costs only include the necessary investment to manufacture one GJ (LHV) of biomethane, i.e., it does not include tax, duties, profits, or marketing costs. Table 14 suggests that the operating and maintenance costs of a biogas upgrading plant based on physical absorbing ILs play a

Table 14. Biomethane Production Costs for the Selected Process Concepts

	$[C_2MIm][Tf_2N]$	$[C_6MIm][Tf_2N]$	$[P_{66614}][Tf_2N]$
capital (\$ GJ^{-1})	5.83	6.25	7.30
O&M (\$ GJ^{-1})	3.35	3.53	4.02
total (\$ GJ^{-1})	9.18	9.78	11.32

significant role in the production costs of biomethane, accounting for around 65% of the total production costs in all cases, and the capital annuity accounts for 35%. The lowest production cost is achieved by $[C_2MIm][Tf_2N]$ at $9.18 per GJ (LHV), followed by $[C_6MIm][Tf_2N]$ and $[P_{66614}][Tf_2N]$ at $9.78 and $11.32 per GJ (LHV), respectively. This is due to the fact that the capital and operating costs for $[C_2MIm][Tf_2N]$ are the lowest of the three concepts considered. Additionally, the production rate of biomethane for $[C_2MIm][Tf_2N]$ is the highest of all process designs.

The process concept based on $[C_2MIm][Tf_2N]$ has the lowest production costs despite the fact that, among the ILs evaluated in this study, it is the one with the lowest absorption capacity. This demonstrates the need of holistic evaluations of ILs for CO_2 capture. These results reveal that parameters such as the physical properties of the IL (heat capacity, viscosity, etc.) and the effect of other gaseous species in the gas stream should also be taken into account, as they were in this study.

5.3.1. Comparison with a MEA Capture Process. For the results above to be put into context, a comparison with existing biogas upgrading processes is essential. The current best practice of biogas upgrading includes a wide range of technologies, such as pressure swing adsorption (PSA), high pressure physical absorption with water or the Selexol solvent, chemical absorption with amines, membrane separation, and cryogenic processes.[68] Given the scope of this study, a fair comparison can only be made with absorption processes that involve either physical or chemical absorption. It was decided to compare the performance of ILs studied in this work with an MEA-based CO_2 capture process. This decision was based on the lack of data regarding the proprietary Selexol solvent when used in biogas upgrading applications and also the fact that high pressure absorption with water is limited to lower flow rates of biogas/flue-gas due to the low CO_2 absorption capacity of water.[68] This last statement is particularly important because this work aims to develop a methodology that is not only suitable for a process that removes CO_2 from biogas but is also applicable to larger applications like postcombustion CO_2 capture from industrial sources, e.g., power plants, refineries, and so forth.

The MEA-based CO_2 capture process has been modeled using the approach reported by Dimitriou et al.[6] The model uses the ENRTL-RK property method in Aspen Plus to estimate thermodynamic and physical properties. An electrolyte calculation option is also used to model the electrolyte solution chemistry as well as the reactions that take place in the absorber and stripper. To allow for fair comparisons, the MEA process assumes the same flow rate and conditions for biogas (composition, temperature, and pressure), dimensions of the absorber, type of packing, and composition of the upgraded biomethane (95 vol %) as the three IL CO_2 capture plants examined in the previous sections.

Table 15 shows the total capital investment and O&M expenditure of the processes using ILs and the MEA process. In all cases, the process designs using ILs have higher capital costs than the MEA process by a factor of 3. This is due to the additional equipment costs related to the compression of biogas in the ionic liquid processes. Additionally, the solvent costs are considerably higher when using ILs. As for the O&M expenditure, the MEA process results in lower costs than those of the processes using ILs.

Figure 5 shows the production costs of all IL-based processes as well as the MEA process. The lowest biomethane production

Table 15. IL-MEA Comparison of TCI and Operating Costs of Biogas Upgrading Processes

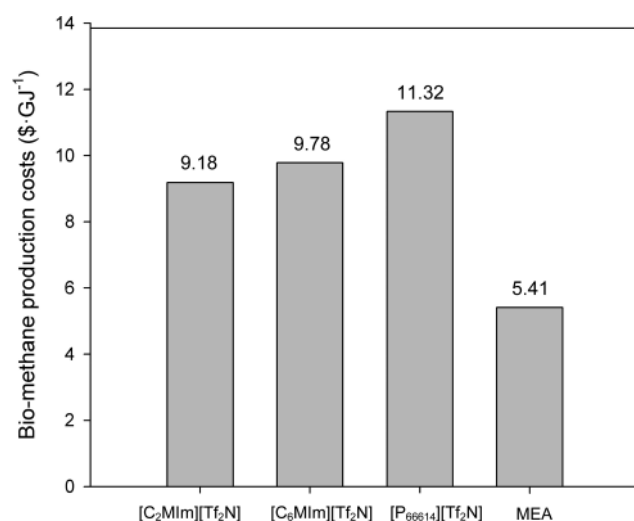|	CAPEX (M$)	OPEX (M$)
$[C_2MIm][Tf_2N]$	15.18	3.10
$[C_6MIm][Tf_2N]$	15.28	3.18
$[P_{66614}][Tf_2N]$	15.10	3.23
MEA	4.45	2.59

Figure 5. Biomethane production costs for the different process concepts.

costs are achieved by the MEA process with a value of $5.41 GJ^{-1} (LHV), which is 41−52% lower than those of the processes using ILs. These results encourage further research in this area, especially taking into account that the ILs evaluated in this work absorb the CO_2 physically as opposed to MEA, which absorbs the CO_2 mainly through chemical interactions. Additionally, the current selling price of ILs is expected to decrease in the future as production and consumption of ILs become more widespread in industry. The effect of IL selling price is studied in the sensitivity analysis in section 5.4.

5.4. Sensitivity Analysis. This section investigates the effect of several important technical and economic parameters on the biomethane production costs. The parameters investigated are absorber pressure, capital investment, plant operating hours, loan interest rate, plant lifespan, electricity price, and IL cost. Figure 6 shows how the absorber pressure affects the biomethane production costs. When the absorber is operated at 20 bar, the production costs decrease to $8.86, $9.33, and $11.11 GJ^{-1} for $[P_{66614}][Tf_2N]$, $[C_6MIm][Tf_2N]$, and $[C_2MIm][Tf_2N]$, respectively; this represents a decrease between 2 and 5% compared to the base case costs. If the operating pressure of the absorber is further reduced to 10 bar, the productions costs of the biomethane increase between 5 and 13% with respect to the production costs at 20 bar and between 1 and 10% with respect to the production costs at 30 bar. As a result, it can be concluded that, in all cases, the minimum production cost of the biomethane is when the absorber is operated at 20 bar. The reason for this minimum is that there is a trade-off between the higher absorption capacity of the ILs at 30 bar, which reduces the amount of fluid needed, and the higher electricity consumption and equipment costs associated with operating the absorber at such high pressure. If the absorber pressure is further reduced to 10 bar, the savings
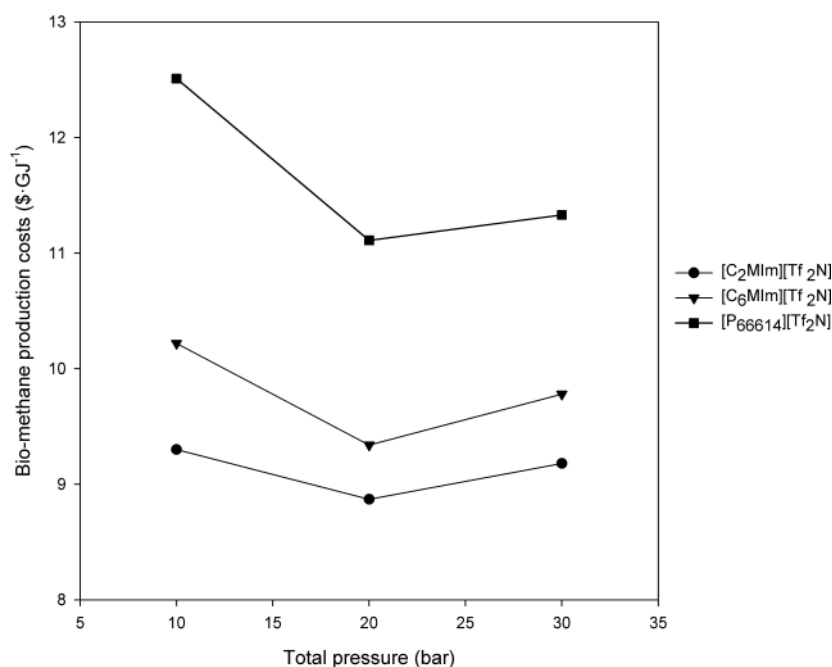
Figure 6. Sensitivity of the biomethane production costs to variations in the absorption pressure.

in electricity and equipment costs related to a high pressure operation are offset by the dramatic increase in the IL fluid needed to produce biomethane at 95 mol %.

For the other parameters, the sensitivity analysis was performed by changing each parameter at a time by ±30% of its base case value; however, the plant operating hours were varied by ±9.5% because the number of hours in a year (8760 h) cannot be exceeded. The results from the three process concepts studied are shown in Figure 7, where longer bars indicate a higher degree of deviation from the base case value.

In all cases, biomethane production costs are most sensitive to plant operating hours because variations of just ±9.5% in this parameter results in a nearly identical effect to varying the capital costs by ±30%. Therefore, these types of plants should be operated with the minimum periods of shutdown possible to achieve significantly lower biomethane production costs.

Production costs are also highly sensitive to variations in capital expenditure. A capital investment variation of ±30% results in the production costs varying by ±10% in all cases. This is an important result because errors of up to ±30% are common in capital investment estimates.[6]

The loan interest rate is the third most sensitive parameter, and fluctuations of ±30% result in the production costs varying by up to 7% in all cases. Interest rates affect the annuity of the capital investment, and therefore, efforts should be made at the early stages of the project development to agree to a fixed rate with the lender throughout the lifespan of the project so that unexpected fluctuation can be avoided. Finally, the biomethane production costs are less sensitive to the plant life of the project, the electricity price, and the IL cost. However, fluctuations in these parameters should not be underestimated because they could significantly affect the production costs.

6. CONCLUSIONS

This study has considered three ILs that absorb CO_2 physically for a biogas upgrading application. Each of the processes developed employs a different IL, keeping the design of the process identical and differing only in the type of IL used. All

three process designs are pressure-swing regenerative processes, whereby the IL absorbs CO_2 in an absorption column at high pressure, and it is regenerated in a flash evaporator at low pressure. A techno-economic assessment of the three evaluated process concepts has been carried out using Aspen Plus and Aspen process economic analyzer (APEA), which has been enabled to determine the most promising IL in terms of energy efficiency and biomethane production cost.

The overall plant efficiency and biomethane production costs associated with the different process concepts range from 71 to 86% and \$9.18−11.32 GJ^{-1} (LHV), respectively. The process using $[C_2MIm][Tf_2N]$ results in the highest plant efficiency and lowest production costs, even though it has the lowest CO_2 absorption capacity of the three ILs evaluated. This is due to the fact that the process using $[C_2MIm][Tf_2N]$ is associated with lower capital and operating costs as well as higher biomethane production rate compared to the other two cases. These results suggest that, to assess the performance of an IL for CO_2 capture, process simulation studies are of paramount importance because only such studies can provide insights on relevant technical and economic parameters related to the commissioning and operation of the plant. The sensitivity analysis shows that the production costs are lowest when the plants are operated at 20 bar. Increasing the pressure to 30 bar increases the absorption capacity of the ILs at the expense of a dramatic escalation in the capital investment and electricity consumption of the biogas compressor. In contrast, reducing the absorption pressure to 10 bar results in significantly lower absorption capacity of the ILs. The biomethane production costs are also sensitive to fluctuations in the plant operating hours, capital investment, and interest rate.

This work has also revealed that production costs of biomethane using ILs as physical absorbents are 40−51% higher than a same-scale MEA-based CO_2 capture process. This encourages further research in the area, which should focus on finding ILs that absorb CO_2 at moderate pressures and are easy to regenerate, ideally only by pressure swing without heating. Our results show that the simulation methodology developed in
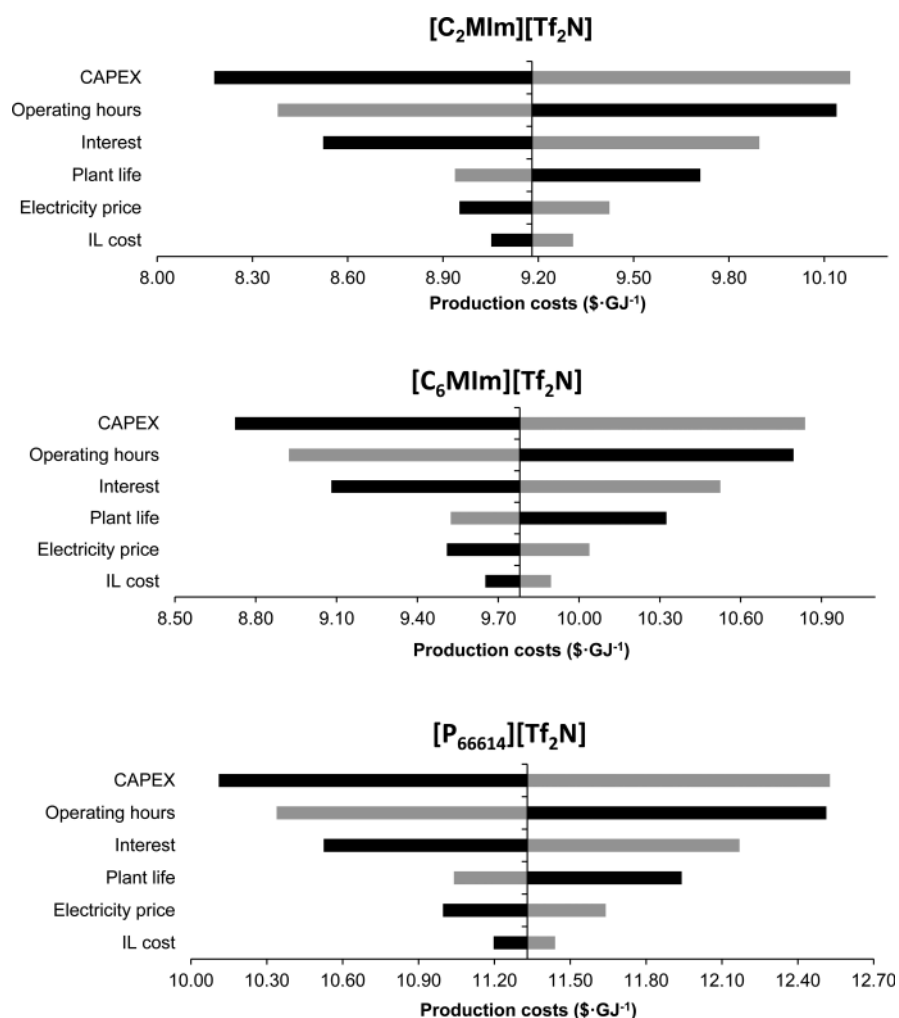
Figure 7. Sensitivity of biomethane production costs to variations of selected technical and economic parameters (all parameters are varied by +30% (gray) and −30% (black), except for the plant operating hours, which are varied by ±9.5%). The vertical line in the graphs represents the production cost of the base case for the three ionic liquids.

this study is a robust tool for predicting plant efficiencies and production costs of large-scale CO_2 capture processes using ILs without relying on gas solubility experimental data.

■ ASSOCIATED CONTENT

ⓢ Supporting Information

The Supporting Information is available free of charge on the ACS Publications website at DOI: 10.1021/acs.energy-fuels.6b00364.

> Pure component and CPIG parameters, ideal gas heat capacity polynomial coefficients, DIPPR and Andrade equation coefficients, σ profile parameters, and predicted relative to experimental data comparisons (PDF)

■ AUTHOR INFORMATION

Corresponding Authors
*E-mail: p.garciagutierrez@sheffield.ac.uk.
*E-mail: johan.jacquemin@qub.ac.uk.

Notes
The authors declare no competing financial interest.

■ ACKNOWLEDGMENTS

■ REFERENCES

(1) Appels, L.; Lauwers, J.; Degrève, J.; Helsen, L.; Lievens, B.; Willems, K.; Dewil, R. Anaerobic digestion in global bio-energy production: Potential and research challenges. *Renewable Sustainable Energy Rev.* **2011**, *15* (9), 4295−4301.
(2) Rajendran, K.; Kankanala, H. R.; Martinsson, R.; Taherzadeh, M. J. Uncertainty over techno-economic potentials of biogas from municipal solid waste (MSW): A case study on an industrial process. *Appl. Energy* **2014**, *125*, 84−92.
(3) Starr, K.; Gabarrell, X.; Villalba, G.; Talens, L.; Lombardi, L. Life cycle assessment of biogas upgrading technologies. *Waste Manage.* **2012**, *32* (5), 991−999.
(4) Poeschl, M.; Ward, S.; Owende, P. Environmental impacts of biogas deployment − Part II: life cycle assessment of multiple

production and utilization pathways. *J. Cleaner Prod.* **2012**, *24*, 184–201.

(5) Ryckebosch, E.; Drouillon, M.; Vervaeren, H. Techniques for transformation of biogas to biomethane. *Biomass Bioenergy* **2011**, *35* (5), 1633–1645.

(6) Dimitriou, I.; García-Gutiérrez, P.; Elder, R. H.; Cuéllar-Franca, R. M.; Azapagic, A.; Allen, R. W. K. Carbon dioxide utilisation for production of transport fuels: process and economic analysis. *Energy Environ. Sci.* **2015**, *8* (6), 1775–1789.

(7) Notz, R. J.; Tönnies, I.; McCann, N.; Scheffknecht, G.; Hasse, H. CO_2 Capture for Fossil Fuel-Fired Power Plants. *Chem. Eng. Technol.* **2011**, *34* (2), 163–172.

(8) Rubin, E. S.; Mantripragada, H.; Marks, A.; Versteeg, P.; Kitchin, J. The outlook for improved carbon capture technology. *Prog. Energy Combust. Sci.* **2012**, *38* (5), 630–671.

(9) Zhu, L.; Schade, G. W.; Nielsen, C. J. Real-Time Monitoring of Emissions from Monoethanolamine-Based Industrial Scale Carbon Capture Facilities. *Environ. Sci. Technol.* **2013**, *47* (24), 14306–14314.

(10) Kittel, J.; Idem, R.; Gelowitz, D.; Tontiwachwuthikul, P.; Parrain, G.; Bonneau, A. Corrosion in MEA units for CO_2 capture: Pilot plant studies. *Energy Procedia* **2009**, *1* (1), 791–797.

(11) Abu-zahra, M. R. M.; Feron, P. H. M.; Versteeg, G. F. CO_2 capture from power plants Part I. A parametric study of the technical performance based on monoethanolamine. *Int. J. Greenhouse Gas Control* **2007**, *1*, 37–46.

(12) Zhang, X.; Zhang, X.; Dong, H.; Zhao, Z.; Zhang, S.; Huang, Y. Carbon capture with ionic liquids: overview and progress. *Energy Environ. Sci.* **2012**, *5* (5), 6668–6681.

(13) Brennecke, J. F.; Gurkan, B. E. Ionic Liquids for CO_2 Capture and Emission Reduction. *J. Phys. Chem. Lett.* **2010**, *1* (24), 3459–3464.

(14) Reddy, R. G. Novel applications of ionic liquids in materials processing. *Journal of Physics: Conference Series* **2009**, *165* (1), 012076.

(15) Lee, B.; Lin, S. Screening of ionic liquids for CO_2 capture using the COSMO-SAC model. *Chem. Eng. Sci.* **2015**, *121*, 157–168.

(16) Basha, O. M.; Heintz, Y. J.; Keller, M. J.; Luebke, D. R.; Resnik, K. P.; Morsi, B. I. Development of a Conceptual Process for Selective Capture of CO_2 from Fuel Gas Streams Using Two TEGO Ionic Liquids as Physical Solvents. *Ind. Eng. Chem. Res.* **2014**, *53* (8), 3184–3195.

(17) Basha, O. M.; Keller, M. J.; Luebke, D. R.; Resnik, K. P.; Morsi, B. I. Development of a Conceptual Process for Selective CO_2 Capture from Fuel Gas Streams Using [hmim][Tf₂N] Ionic Liquid as a Physical Solvent. *Energy Fuels* **2013**, *27* (7), 3905–3917.

(18) Eisinger, R. S.; Keller, G. E. Process for CO_2 Capture Using Ionic Liquid That Exhibits Phase Change. *Energy Fuels* **2014**, *28* (11), 7070–7078.

(19) Shiflett, M. B.; Drew, D. W.; Cantini, R. a.; Yokozeki, A. Carbon Dioxide Capture Using Ionic Liquid 1-Butyl-3-methylimidazolium Acetate. *Energy Fuels* **2010**, *24* (10), 5781–5789.

(20) Styring, P.; Jansen, D.; de Coninck, H.; Reith, H.; Amstrong, K. *Carbon Capture and Utilisation in the Green Economy*; CO2Chem: Sheffield, UK, 2011.

(21) Ferro, V. R.; Ruiz, E.; de Riva, J.; Palomar, J. Introducing process simulation in ionic liquids design/selection for separation processes based on operational and economic criteria through the example of their regeneration. *Sep. Purif. Technol.* **2012**, *97*, 195–204.

(22) Bedia, J.; Ruiz, E.; de Riva, J.; Ferro, V. R.; Palomar, J.; Rodriguez, J. J. Optimized Ionic Liquids for Toluene Absorption. *AIChE J.* **2013**, *59*, 1648–1656.

(23) Ruiz, E.; Ferro, V. R.; de Riva, J.; Moreno, D.; Palomar, J. Evaluation of ionic liquids as absorbents for ammonia absorption refrigeration cycles using COSMO-based process simulations. *Appl. Energy* **2014**, *123*, 281–291.

(24) Ferro, V. R.; de Riva, J.; Sanchez, D.; Ruiz, E.; Palomar, J. Conceptual design of unit operations to separate aromatic hydrocarbons from naphtha using ionic liquids. COSMO-based process simulations with multi-component "real" mixture feed. *Chemical Engineering Research & Design* **2015**, *94*, 632–647.

(25) de Riva, J.; Ferro, V. R.; Moreno, D.; Diaz, I.; Palomar, J. Aspen Plus supported conceptual design of the aromatic−aliphatic separation from low aromatic content naphtha using 4-methyl-N-butylpyridinium tetrafluoroborate ionic liquid. *Fuel Process. Technol.* **2016**, *146*, 29–38.

(26) Hagen, M.; Polman, E.; Myken, A.; Jensen, J.; Jönsson, O.; Dahl, A. Adding gas from biomass to the gas grid, Contract No: XVII/4.1030/Z/99−412, Final Report; Malmö, Sweden, 2001

(27) REA. Minworth Sewage Treatment Works - A case study for Biomethane to Grid, 2013. http://www.r-e-a.net/images/upload/e v e n t s 1 3 3 5 - S i m o n F a r r i s - SevernTrentMinworthUKBiomethaneDay2013.pdf (accessed Nov. 21, 2015).

(28) Cadena, C.; Anthony, J. L.; Shah, J. K.; Morrow, T. I.; Brennecke, J. F.; Maginn, E. J. Why Is CO_2 so soluble in imidazolium-based ionic liquids? *J. Am. Chem. Soc.* **2004**, *126* (16), 5300–8.

(29) Anthony, J. L.; Anderson, J. L.; Maginn, E. J.; Brennecke, J. F. Anion effects on gas solubility in ionic liquids. *J. Phys. Chem. B* **2005**, *109* (13), 6366–74.

(30) Lei, Z.; Dai, C.; Chen, B. Gas solubility in ionic liquids. *Chem. Rev.* **2014**, *114*, 1289–1326.

(31) Sumon, K. Z.; Henni, A. Ionic liquids for CO_2 capture using COSMO-RS: Effect of structure, properties and molecular interactions on solubility and selectivity. *Fluid Phase Equilib.* **2011**, *310* (1−2), 39–55.

(32) NIST, 2013. Ionic Liquids Database - ILThermo (v2.0). http://ilthermo.boulder.nist.gov/ (accessed Oct. 2, 2015).

(33) Palomar, J.; Gonzalez-Miquel, M.; Polo, A.; Rodriguez, F. Understanding the physical absorption of CO_2 in ionic liquids using the COSMO-RS method. *Ind. Eng. Chem. Res.* **2011**, *50*, 3452–3463.

(34) Zhang, X.; Liu, Z.; Wang, W. Screening of ionic liquids to capture CO_2 by COSMO-RS and experiments. *AIChE J.* **2008**, *54* (10), 2717–2728.

(35) Aspen Technology. Aspen Physical Property System - Physical Property Models; Burlington, USA, 2013.

(36) *COSMOlogic*. COSMOtherm: Predicting Solutions since 1999, 2015. http://www.cosmologic.de/products/cosmotherm.html (accessed Dec. 1, 2015).

(37) *Aspen Technology*. Aspen Plus User Guide; Burlington, USA, 2000.

(38) Koch-Glitsch. Metal Random Packing, 2015. http://www.koch-glitsch.com/Document%20Library/KGMRP-02.pdf (accessed Mar. 31, 2016).

(39) Sulzer. Random Packing. From competitive products to advanced solutions, 2015. http://www.sulzer.com/en/-/media/Documents/ProductsAndServices/Separation_Technology/Distillation_Absorption/Brochures/Random_Packing.pdf (accessed Mar. 31, 2016).

(40) Sønderby, T. L.; Carlsen, K. B.; Fosbol, P. L.; Kiorboe, L. G.; von Solms, N. A new pilot absorber for CO_2 capture from flue gases: Measuring and modelling capture with MEA solution. *Int. J. Greenhouse Gas Control* **2013**, *12*, 181–192.

(41) Billet, R.; Schultes, M. Predicting mass transfer in packed columns. *Chem. Eng. Technol.* **1993**, *16* (1), 1–9.

(42) Coulson, J. M.; Richardson, J. F.; Backhurst, J. R.; Harker, J. H. *Coulson and Richardson's Chemical Engineering: Fluid Flow, Heat Transfer and Mass Transfer v. 1*, 5th ed., Butterworth-Heinemann Ltd.: Oxford, UK, 1995.

(43) Britt, H.; Luecke, R. The Estimation of Parameters in a Non-linear, Implicit Model. *Technometrics* **1973**, *15* (2), 233–247.

(44) Paulechka, Y. U.; Blokhin, A. V.; Kabo, G. J.; Strechan, A. A. Thermodynamic properties and polymorphism of 1-alkyl-3-methyl-imidazolium bis(triflamides). *J. Chem. Thermodyn.* **2007**, *39* (6), 866–877.

(45) Blokhin, A. V.; Paulechka, Y. U.; Kabo, G. J. Thermodynamic Properties of [C₆mim][NTf₂] in the Condensed State. *J. Chem. Eng. Data* **2006**, *51* (4), 1377–1388.

(46) Ferreira, A. G. M.; Simões, P. N.; Ferreira, A. F.; Fonseca, M. A.; Oliveira, M. S. A.; Trino, A. S. M. Transport and thermal properties of

quaternary phosphonium ionic liquids and IoNanofluids. *J. Chem. Thermodyn.* **2013**, *64*, 80−92.

(47) Jacquemin, J.; Husson, P.; Majer, V.; Costa Gomes, M. F. Influence of the Cation on the Solubility of CO_2 and H_2 in Ionic Liquids Based on the Bis(trifluoromethylsulfonyl)imide Anion. *J. Solution Chem.* **2007**, *36* (8), 967−979.

(48) Widegren, J. A.; Magee, J. W. Density, Viscosity, Speed of Sound, and Electrolytic Conductivity for the Ionic Liquid 1-Hexyl-3-methylimidazolium Bis(trifluoromethylsulfonyl)imide and Its Mixtures with Water. *J. Chem. Eng. Data* **2007**, *52* (6), 2331−2338.

(49) Neves, C. M. S. S.; Carvalho, P. J.; Freire, M. G.; Coutinho, J. A. P. Thermophysical properties of pure and water-saturated tetradecyltrihexylphosphonium-based ionic liquids. *J. Chem. Thermodyn.* **2011**, *43* (6), 948−957.

(50) Schreiner, C.; Zugmann, S.; Hartl, R.; Gores, H. J. Fractional Walden Rule for Ionic Liquids: Examples from Recent Measurements and a Critique of the So-Called Ideal KCl Line for the Walden Plot. *J. Chem. Eng. Data* **2010**, *55* (5), 1784−1788.

(51) SIGMA-ALDRICH. Sigma-Aldrich catalogue, 1995. http://www.sigmaaldrich.com/united-kingdom.html (accessed Apr. 3, 2015).

(52) Valderrama, J. O.; Rojas, R. E. Critical Properties of Ionic Liquids. Revisited. *Ind. Eng. Chem. Res.* **2009**, *48*, 6890−6900.

(53) Ahlrichs, R.; Bär, M.; Häser, M.; Horn, H.; Kölmel, C. Electronic structure calculations on workstation computers: The program system turbomole. *Chem. Phys. Lett.* **1989**, *162* (3), 165−169.

(54) Weigend, F.; Häser, M. RI-MP2: first derivatives and global consistency. *Theor. Chem. Acc.* **1997**, *97* (1), 331−340.

(55) Talaty, E. R.; Raja, S.; Storhaug, V. J.; Dölle, A.; Carper, W. R. Raman and Infrared Spectra and ab Initio Calculations of C2-C4MIm Imidazolium Hexafluorophosphate Ionic Liquids. *J. Phys. Chem. B* **2004**, *108* (35), 13177−13184.

(56) Carvalho, P. J.; Álvarez, V. H.; Machado, J. J. B.; Pauly, J.; Daridon, J.-L.; Marrucho, I. M.; Coutinho, J. A. P. High pressure phase behavior of carbon dioxide in 1-alkyl-3-methylimidazolium bis-(trifluoromethylsulfonyl)imide ionic liquids. *J. Supercrit. Fluids* **2009**, *48* (2), 99−107.

(57) Liu, X.; Afzal, W.; Prausnitz, J. M. Solubilities of small hydrocarbons in tetrabutylphosphonium bis(2,4,4-trimethylpentyl) phosphinate and in 1-ethyl-3-methylimidazolium bis-(trifluoromethylsulfonyl)imide. *Ind. Eng. Chem. Res.* **2013**, *52*, 14975−14978.

(58) Zubeir, L. F.; Romanos, G. E.; Weggemans, W. M. A.; Iliev, B.; Schubert, T. J. S.; Kroon, M. C. Solubility and Diffusivity of CO_2 in the Ionic Liquid 1-Butyl-3-methylimidazolium Tricyanomethanide within a Large Pressure Range (0.01 to 10 MPa). *J. Chem. Eng. Data* **2015**, *60* (6), 1544.

(59) Kumełan, J.; Pérez-Salado Kamps, Á.; Tuma, D.; Maurer, G. Solubility of the Single Gases Methane and Xenon in the Ionic Liquid [hmim][Tf_2N]. *Ind. Eng. Chem. Res.* **2007**, *46* (24), 8236−8240.

(60) Carvalho, P. J.; Álvarez, V. H.; Marrucho, I. M.; Aznar, M.; Coutinho, J. A. P. High carbon dioxide solubilities in trihexyltetradecylphosphonium-based ionic liquids. *J. Supercrit. Fluids* **2010**, *52* (3), 258−265.

(61) Manan, N. A.; Hardacre, C.; Jacquemin, J.; Rooney, D. W.; Youngs, T. G. A. Evaluation of Gas Solubility Prediction in Ionic Liquids using COSMOthermX. *J. Chem. Eng. Data* **2009**, *54* (7), 2005−2022.

(62) Peters, M. S.; Timmerhaus, K. D.; West, R. E. Plant design and economics for chemical engineers, 5th ed.; McGraw-Hill: New York, 2004.

(63) Aspen Technology. Aspen Process Economic Analyzer - User Guide; Burlington, USA, 2012.

(64) OFGEM. Non-Domestic Renewable Heat Incentive (RHI), 2015. https://www.ofgem.gov.uk/environmental-programmes/non-domestic-renewable-heat-incentive-rhi (accessed July 2, 2015).

(65) Ferro, V. R.; Ruiz, E.; de Riva, J.; Palomar, J. Introducing process simulation in ionic liquids design/selection for separation processes based on operational and economic criteria through the example of their regeneration. *Sep. Purif. Technol.* **2012**, *97*, 195−204.

(66) Meindersma, G. W.; de Haan, A. B. Conceptual process design for aromatic/aliphatic separation with ionic liquids. *Chem. Eng. Res. Des.* **2008**, *86* (7), 745−752.

(67) Wasserscheid, P., Welton, T., Eds. Outlook. In *Ionic Liquids in Synthesis*, 2nd ed.; WILEY-VCH Verlag GmbH & Co.: Weinheim, Germany, 2008; pp 689−704.

(68) Person, M. Evaluation of upgrading techniques for biogas. Swedish Gas Center, Report SGC 142; Lund, Sweden, 2003.